

# A Validation of Causal Dynamical Triangulations

Rajesh Kommu\*

*Department of Physics  
University of California  
Davis, CA 95616  
USA*

November 3, 2011

## Abstract

The Causal Dynamical Triangulation (CDT) approach to quantum gravity is a lattice approximation to the gravitational path integral. Developed by Ambjørn, Jurkiewicz and Loll, it has yielded some important results, notably the emergence of classical spacetime and short scale dimensional reduction. However, virtually all the results reported so far have been based on a single computer code. In this paper we present the first completely independent verification of the CDT algorithm, and report the successful reproduction of the emergence of classical spacetime and smooth reduction in the spectral dimension of the 2+1 and 3+1 dimensional spacetimes.

## 1 Introduction

The Causal Dynamical Triangulations (CDT) approach to quantum gravity has emerged as a breath of fresh air in the effort to quantize gravity. In CDT, developed by Ambjørn, Jurkiewicz and Loll [1, 2, 3, 4], we have an attempt at quantizing gravity that relies solely on ideas and techniques that have been known to physicists for quite some time — path integrals, causality, simplicial manifolds, finite-size scaling effects, etc. The formulation of CDT, while being extremely straightforward, has yielded some important results, such as the *emergence* of classical spacetime and dimensional reduction of spacetimes at short distances.

So far, however, all the results that have been reported for CDT have either come from the original group headed by Ambjørn, Jurkiewicz and Loll or from groups that have used the code or data sets from the original group. In this paper, we present the first independent verification of the CDT algorithm, using code developed from scratch in a completely independent fashion. We have been able to reproduce the important results reported for CDT and set the stage for further results, which will be reported elsewhere [5, 6, 7].

The outline of this paper is as follows. In section 2 we present a brief overview of the Causal Dynamical Triangulation approach. Readers interested in greater detail should refer to [2] and [3]. In section 3 we describe our CDT implementation, at a fairly high level. Finally, in section 4, we present the results from our simulation.

---

\*kommu@physics.ucdavis.edu

## 2 Causal Dynamical Triangulations

CDT is based on the gravitational path integral

$$G(\mathbf{g}_i, \mathbf{g}_f; t_i, t_f) = \int \mathcal{D}[g] e^{iS_{EH}[g]} \quad (1)$$

where

$$S_{EH}[g] = \frac{1}{16\pi G} \int d^n x \sqrt{-g} (R - 2\Lambda) \quad (2)$$

is the Einstein-Hilbert action. Here  $\mathbf{g}_i$  and  $\mathbf{g}_f$  are the spatial metrics on the initial and final slice and  $g$  represents all possible (spacetime) metrics that satisfy the initial and final conditions. By all possible metrics, we mean metrics that are not related to each other by diffeomorphisms. To define the action in the path integral, CDT uses Regge calculus [8] as its starting point. The basic idea of Regge calculus is to approximate a smooth manifold (for example spacetime) with a piecewise linear manifold, with curvature restricted to subspaces of co-dimension two.

The geometrical objects used to approximate  $d$ -dimensional manifolds are  $d$ -simplices, which consist of  $(d-1)$ -dimensional faces,  $(d-2)$ -dimensional hinges or “bones” (on which the curvature of the manifold resides), and so on down to 0-dimensional simplices (points). A  $d$ -simplex has  $d+1$  points.

For manifolds without a boundary, a discrete version of the Einstein-Hilbert action can be formulated using [8]

$$\int d^n x \sqrt{-g} R \rightarrow 2 \sum_{\text{hinges } h} V_h \delta_h \quad (3)$$

$$\int d^n x \sqrt{-g} \rightarrow \sum_d V_d \quad (4)$$

to get

$$S_R = \frac{1}{8\pi G} \sum_h V_h \delta_h - \frac{\Lambda}{8\pi G} \sum_d V_d \quad (5)$$

where  $V_h$  is the volume of a hinge,  $V_d$  is the volume of a top level  $d$ -simplex, and  $\delta_h$  is the deficit angle at  $h$ .

CDT assumes globally hyperbolic spacetimes. The existence of Cauchy hypersurfaces enables us to use  $d$ -simplices that span adjacent spatial slices as the building blocks for our  $d$ -dimensional spacetimes. A time-like  $(p, q)$   $d$ -simplex, where  $p+q = d+1$ , has  $p$  points on the lower time slice and  $q$  points on the adjacent higher time slice. For a space-like simplex, all points are on the same spatial slice. No space-like  $d$ -simplices are present in  $d$ -dimensional spacetimes. But both space-like and time-like types of lower dimensional simplices are present in the spacetime. The simplicial building blocks in CDT have an inherent causal structure built into them. To preserve this causal structure, CDT does not allow topology changes of the spatial slices.

The lengths of the space-like and time-like links (1-simplices) are defined as

$$l_{space}^2 = a^2, l_{time}^2 = -\alpha a^2, \alpha > 0 \quad (6)$$

where  $a$  is the lattice spacing and  $\alpha$  is the asymmetry parameter. In 2+1 dimensions, we have three types of 3-simplices, denoted by  $(1, 3)$ ,  $(2, 2)$  and  $(3, 1)$ . In 3+1 dimensions, we have four types of 4-simplices, denoted by  $(1, 4)$ ,  $(2, 3)$ ,  $(3, 2)$  and  $(4, 1)$ . The volume of each type of simplex and the dihedral angles subtended between the faces of these simplices are given in [2]. Using these, we can

formulate the Lorentzian version of the Regge action in  $d = 3, 4$  as

$$\begin{aligned}
S = & \frac{1}{8\pi G} \sum_{\substack{\text{space-like} \\ \text{hinges}, h}} \text{Vol}(h) \frac{1}{i} \left( 2\pi - \sum_{\substack{d\text{-simplices} \\ \text{at } h}} \Theta \right) \\
& + \frac{1}{8\pi G} \sum_{\substack{\text{time-like} \\ \text{hinges}, h}} \text{Vol}(h) \left( 2\pi - \sum_{\substack{d\text{-simplices} \\ \text{at } h}} \Theta \right) \\
& - \frac{\Lambda}{8\pi G} \sum_{\substack{\text{time-like} \\ d\text{-simplices}, d}} \text{Vol}(d)
\end{aligned} \tag{7}$$

where  $\Theta$  is the dihedral angle subtended at the hinge  $h$ . Equation (7) is a reformulation of (5) with space-like and time-like simplices distinguished.

In CDT, Wick rotation is defined as [2]

$$\alpha \mapsto -\alpha, \alpha > \frac{1}{2} (d=3), \alpha > \frac{7}{12} (d=4) \tag{8}$$

This leads to a pure imaginary value for the action. The gravitational path integral (1) in CDT is replaced by a sum over distinct triangulations

$$\int \mathcal{D}[g] e^{iS} \rightarrow \sum_T \frac{1}{C(T)} e^{iS(T)} \tag{9}$$

where  $C(T)$  is the order of the automorphism group of the triangulation.

The Wick rotated action<sup>1</sup> for a triangulation in 2+1 dimensions is given by

$$S^{(3)} = i(-\kappa_0 N_0 + \kappa_3 N_3) \tag{10}$$

where

$$\kappa_0 = \frac{1}{4G}, \kappa_3 = \frac{\Lambda}{48\sqrt{2}\pi G} + \frac{1}{4G} \left( \frac{3}{\pi} \cos^{-1}(1/3) - 1 \right) \tag{11}$$

and  $N_0, N_3$  are the number of 0-simplices and 3-simplices, respectively. Equation (10) can be derived from (7) by substituting the appropriate expressions for the simplex volumes and dihedral angles, using topological identities for (2+1)-dimensional Lorentzian triangulations [2] and then performing a Wick rotation (8). The topological identities eliminate all but two of the bulk variables  $N_0 \cdots N_d$ .

Substituting the Wick rotated action in (9) gives us the partition function:

$$Z = \sum_T \exp(\kappa_0 N_0 - \kappa_3 N_3) \tag{12}$$

A similar procedure in 3+1 dimensions leads to the Wick rotated action

$$S^{(4)} = i \left( -(\kappa_0 + 6\Delta) N_0 + \kappa_4 N_4 + \Delta(2N_4^{(4,1)} + N_4^{(3,2)}) \right) \tag{13}$$

and the corresponding partition function

$$Z = \sum_T \exp \left( (\kappa_0 + 6\Delta) N_0 - \kappa_4 N_4 - \Delta(2N_4^{(4,1)} + N_4^{(3,2)}) \right) \tag{14}$$

---

<sup>1</sup>Equations (10) and (11) are derived for  $\alpha = -1$ . For  $\alpha \neq -1$  the action will have terms involving  $N_0, N_3^{(3,1)}$  and  $N_3^{(2,1)}$ , where  $N_3^{(3,1)}$  and  $N_3^{(2,2)}$  are the number of (3,1) and (2,2) 3-simplices. However, in 2+1 dimensions, there are only two independent bulk degrees of freedom, so the action still takes the form (10), although with (11) altered. See [2] for details.

where

$$\kappa_0 = \frac{\sqrt{3}}{8G}, \kappa_4 = \frac{\Lambda\sqrt{5}}{768\pi G} + \frac{\sqrt{3}}{8G} \left( \frac{5}{2\pi} \cos^{-1}(1/4) - 1 \right) \quad (15)$$

and  $\Delta$  is a complicated function that depends on  $\alpha$ , with  $\alpha = 1$  corresponding to  $\Delta = 0$ .  $N_4^{(4,1)}$  is the number of  $(4, 1)$  plus  $(1, 4)$  simplices, and  $N_4^{(3,2)}$  is the number of  $(3, 2)$  plus  $(2, 3)$  simplices.

To generate the distinct triangulations required for evaluating the partition function and the expectation value of any observable, the CDT approach uses a set of ergodic moves. An ergodic move applied to a triangulation yields another distinct triangulation, one that is not related to the first one by a diffeomorphism. Ergodicity ensures that we can go from one triangulation to any other triangulation by repeated application of moves. Ergodic moves also preserve the topology of the manifold, as well as the simplicial manifold property. The moves are described in detail in [2].

### 3 Numerical Implementation

In our numerical implementation, each  $d$ -simplex is identified by a unique ID and is stored as a list (containing sublists) of points

```
(ty lo hi (p0 p1 . . . pd) (n0 n1 . . . nd))
```

Here **ty** identifies the type of the simplex  $\text{ty} = 1, 2, \dots, d$ . **lo** and **hi** are the lower and higher time slices spanned by the simplex. The **pis** are the points that make up the simplex, and the **nis** are the IDs of the neighboring simplices. The simplex **nk** is connected on the  $(\text{p0} \dots \text{pd}) - (\text{pk})$  face. The points are used only as unique labels to identify the vertices of a simplex. While we distinguish the points on the lower time slice from the points on the higher time slice, the ordering of the points in any given slice is immaterial.

With this choice for the simplex data structure, it is fairly straightforward to implement the ergodic moves described in detail in [2]. It is essential that the moves maintain the simplicial property of the manifold. This requires that two simplices should be connected across a single face and that a  $(d - 1)$ -simplex should be shared between exactly two  $d$ -simplices.

To generate the distinct triangulations using the ergodic moves, we apply the Metropolis algorithm [9]. The Metropolis algorithm uses a Markov chain that, upon reaching equilibrium, satisfies the following detailed balance condition

$$P(T_1)W(T_1, T_2) = P(T_2)W(T_2, T_1) \quad (16)$$

where  $P(T_i)$  is the probability of being in a particular triangulated geometry  $T_i$  and  $W(T_i, T_j)$  is the transition probability of going from triangulation  $T_i$  to triangulation  $T_j$ . The probability of being in a particular triangulation is proportional to the Boltzmann weight  $e^{-S_E}$ . The detailed balance condition in this case can be written as:

$$\frac{W(T_1, T_2)}{W(T_2, T_1)} = \frac{e^{-S_E(T_2)}}{e^{-S_E(T_1)}} = e^{-\Delta S_E} \quad (17)$$

The simplest choice for the transition probability  $W$  that satisfies this condition is

$$W(T_1, T_2) = \begin{cases} e^{-\Delta S_E}, & \text{if } \Delta S_E > 0 \\ 1, & \text{if } \Delta S_E \leq 0 \end{cases} \quad (18)$$

Thus a move that increases the action may be accepted or rejected, while moves that decrease the action or leave the action unchanged are always accepted.

We initialize the simulation by specifying the number of time slices  $T$  and the total volume of the spacetime. The initialization process starts by triangulating each spatial slice as a  $(d - 1)$ -sphere. The  $t = 0$  and the  $t = T$  slices are identified to enforce the periodic boundary conditions in time. This is done for technical convenience, rather than due to any physical argument. Next, the triangulations on adjacent slices are connected. We then apply the volume increasing subset of the ergodic moves until the total volume reaches the desired target volume.

Once the simulation has been initialized, we have to run simulation for about 100,000 sweeps to thermalize the spacetimes. A sweep is defined as  $N_d$  attempted moves, where  $N_d$  is number of  $d$ -simplices in the spacetime. Thermalization ensures that the system is sufficiently randomized, and has moved away from the highly structured initial conditions. Once thermalization is completed, we start saving spacetimes every 100 sweeps, to build our ensembles.

## 4 Results

### 4.1 Phase Structure

In 2+1 dimensions, the phase structure of the CDT model can be explored by tracking the dependence of an order parameter on coupling constants. The order parameter selected is the ratio of the number of  $(2, 2)$  3-simplices to the total number of 3-simplices in the spacetime:

$$\tau = \frac{N_{22}}{N_3} = \frac{N_{22}}{N_{13} + N_{22} + N_{31}} \quad (19)$$

The dependence of  $\tau$  on the coupling constant is shown in figure 1.

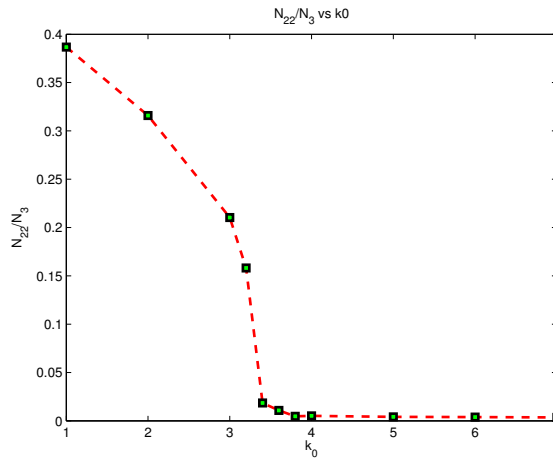


Figure 1:  $\frac{N_{22}}{N_3}$  versus  $\kappa_0$

Figure 1 shows a phase transition, at  $\kappa_0^c \approx 3.3$ . In [3], this phase transition was reported at a value of  $\kappa_0^c \approx 6.6$ . The two results differ by a factor of two, for reasons we do not understand, but the qualitative results are identical. For  $\kappa_0 > \kappa_0^c$ , we observe that the spatial volumes of successive slices is not strongly correlated — spacetime has effectively decoupled into disconnected spatial slices. This is shown in figure 2, where we have a taken a snapshot of a simulation in this decoupled phase.

A snapshot of the simulation in the other phase, characterized by  $\kappa_0 < \kappa_0^c$ , clearly shows the emergence of a well defined, extended geometry phase. This is shown in figure 3. The simulation fluctuates around this extended geometry, a geometry that resembles a classical universe. This classical spacetime *emerges* from the simulation, and was not explicitly specified by us. In this phase,

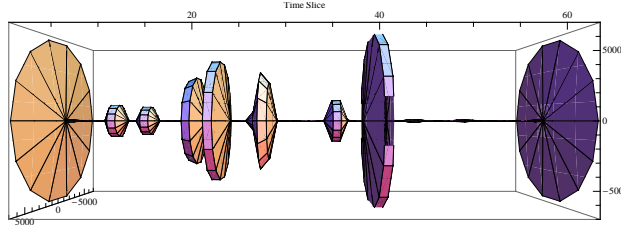


Figure 2: A snapshot of a (2+1)-dimensional spacetime in the decoupled phase.

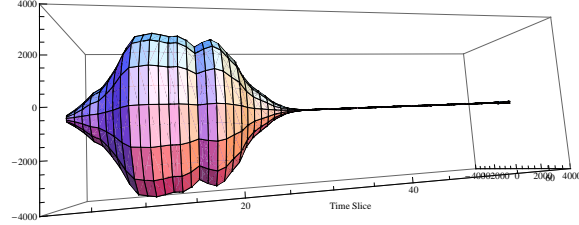


Figure 3: A snapshot of a (2+1)-dimensional spacetime in the extended phase.

the volume of successive spatial slices is strongly correlated, and the path integral is dominated by metrics that are approximate solutions of the Einstein equations.

A thick slice is defined as the portion of spacetime that is bounded by adjacent spatial slices. Thick slices are labelled by half-integer values where, for example, a thick slice labelled by  $t = 1/2$ , is bounded by the spatial slices  $t = 0$  and  $t = 1$ . The volume of a thick slice is defined as the number of  $d$ -simplices in that thick slice. In figures 2 and 3 time is along the horizontal axis. These figures were generated by considering the volumes of the thick slices for half-integer values ranging from  $t = 1/2$  to  $t = T - 1/2$  where  $T$  is total number of time slices. We draw a circle with radius equal to the volume of the slice, and join circles corresponding to adjacent thick slices by linear interpolation. The axial symmetry in these figures is therefore a visualization artefact. Figure 4 shows a typical spatial slice in 2+1 dimensions, embedded in a three dimensional space [6].

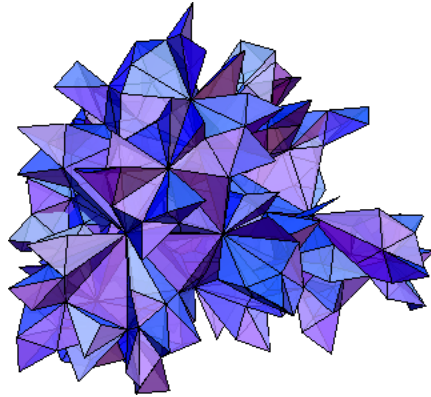


Figure 4: A spatial slice in 2+1 dimensions.

In 3+1 dimensions, while we are not aware of an order parameter analogous to the  $(2 + 1)$ -dimensional case, we do observe three distinct phases, illustrated in figures 5, 6 and 7. All three figures are for spacetimes with  $T = 64$  and  $N_4 = 81920$

Phase A is characterized by a splitting up of the spacetime in small pieces of irregular volume, with each piece not extending beyond a few time slices. In Phase B, all of the spacetime volume collapses into a single piece of minimal extension. Both of these non-physical phases are character-

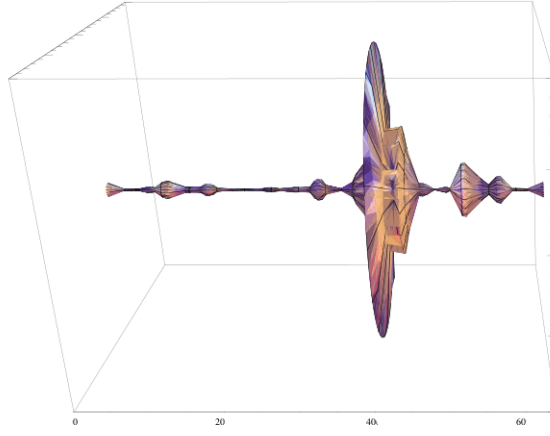


Figure 5: A (3+1)-dimensional spacetime in phase A,  $\kappa_0 = 5.0, \Delta = 0.0, \kappa_4 = 1.01$

ized by a small value for the ratio  $\frac{N_{(3,2)}}{N_4}$ . Phase C is the extended geometric phase, where there is

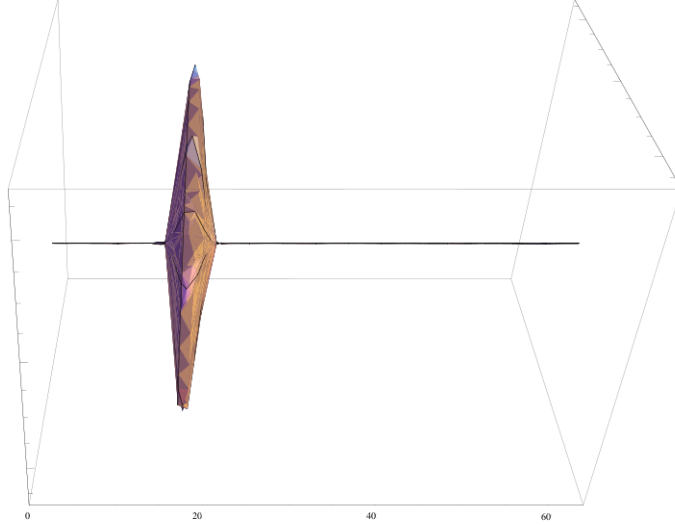


Figure 6: A (3+1)-dimensional spacetime in phase B,  $\kappa_0 = 1.6, \Delta = 0.0, \kappa_4 = 0.65$

a strong correlation between the volumes of successive spatial slices.

## 4.2 Spectral Dimension

One of the major contributions of the CDT approach has been the introduction of the spectral dimension as probe of the properties of spacetime, both on short and long scales.

The diffusion equation for a  $d$ -dimensional manifold with a smooth metric  $g_{\mu\nu}$  is given by [10, 11]

$$\frac{\partial}{\partial \sigma} K_g(\xi, \xi_0; \sigma) = \Delta_g K_g(\xi, \xi_0; \sigma) \quad (20)$$

where  $\sigma$  is the diffusion time,  $\Delta_g = -g^{\mu\nu} \nabla_\mu \nabla_\nu$  is the Laplace operator corresponding to  $g_{\mu\nu}(\xi)$  and  $K_g(\xi, \xi_0; \sigma)$  is the probability density of diffusion from  $\xi_0$  to  $\xi$  in a time  $\sigma$ . The diffusion processes

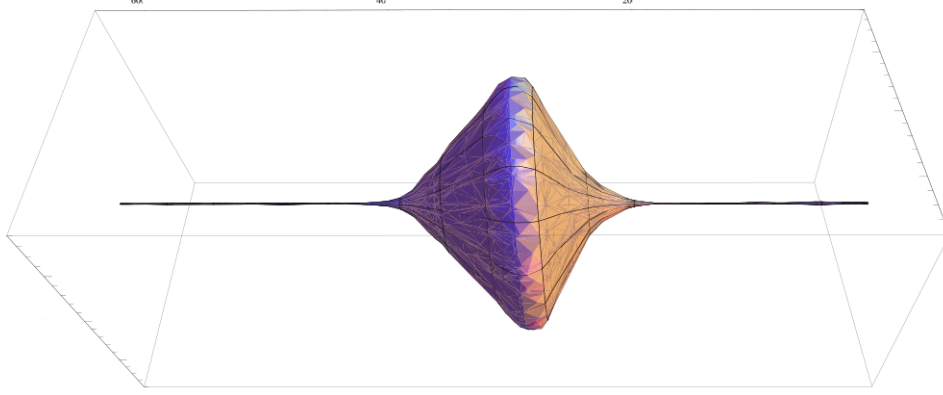


Figure 7: A (3+1)-dimensional spacetime in phase C,  $\kappa_0 = 2.4$ ,  $\Delta = 0.6$ ,  $\kappa_4 = 0.079$

we care about are ones that are initially peaked at a point  $\xi_0$

$$K_g(\xi, \xi_0; \sigma = 0) = \frac{\delta^d(\xi - \xi_0)}{\sqrt{|g|}} \quad (21)$$

Instead of probability density, we measure the return probability, which is defined as

$$P_g(\sigma) = \frac{1}{V} \int_M d^d \xi \sqrt{|g|} K_g(\xi, \xi; \sigma) \quad (22)$$

For a flat space with infinite volume, the solution of equation (20) is [10, 11]

$$K_g(\xi, \xi_0; \sigma) = \frac{e^{-d_g^2(\xi, \xi_0)/4\sigma}}{(4\pi\sigma)^{d/2}} \quad (23)$$

where  $d_g(\xi, \xi_0)$  is the geodesic distance between  $\xi$  and  $\xi_0$ . The return probability for the flat space case is

$$P_g(\sigma) = \frac{1}{\sigma^{d/2}} \quad (24)$$

Taking the logarithmic derivative of the equation (24), we get

$$-2 \frac{d \ln P(\sigma)}{d \ln \sigma} = d \quad (25)$$

This definition of the spectral dimension can be extended to curved and/or finite volume spacetimes, with the addition of finite-size corrections, and allows one to define a generalized dimension on a wide variety of spaces that are not smooth manifolds [12]

In CDT, the spectral dimension [10, 4, 13] of the spacetime is measured by initiating a diffusion process from a randomly selected simplex. A single step in a random walk is generated by moving to randomly selected neighbor. By initiating a large number of walks with  $\sigma$  steps, we can calculate the probability of returning to the starting simplex. The return probability can be then used to compute the spectral dimension.

The spectral dimension vs step size plot for a (2+1)-dimensional spacetime is shown in figure 8. We observe that the spectral dimension demonstrates a smooth transition from a value of about



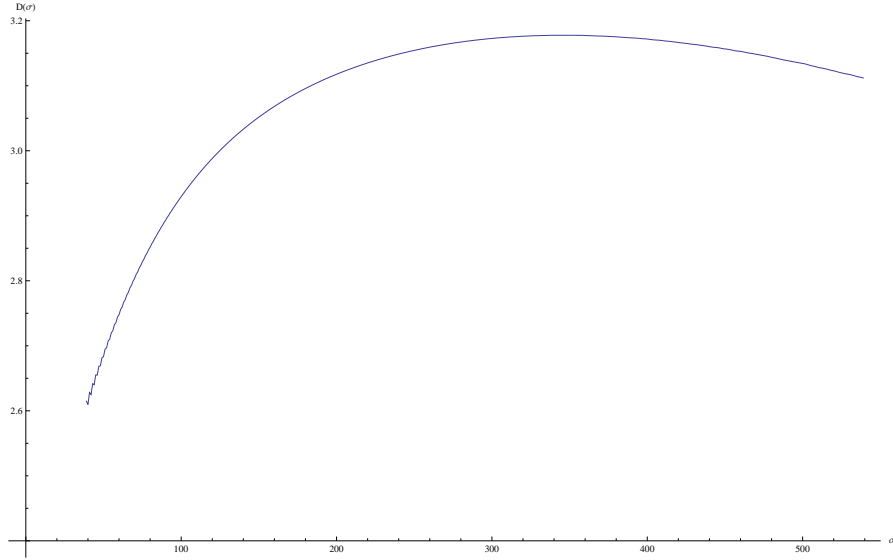


Figure 8: Spectral dimension for a (2+1) spacetime vs  $\sigma$ ,  $N_3 = 80000$ ,  $\kappa_0 = 1.0$

2.4 at short scales up to a value of about 3.0 at larger values of  $\sigma$ , and then starts to fall for  $\sigma$  greater than about 400. Fitting the data to a function of the form  $D(\sigma) = a + \frac{b}{c + \sigma}$  we obtain

$$D(\sigma) = 3.03 - \frac{10.51}{17.87 + \sigma} \quad (26)$$

Fitting the data to  $D(\sigma) = a + be^{-c\sigma}$ , as suggested in [11], we obtain

$$D(\sigma) = 3.19 - 0.97e^{-0.013\sigma} \quad (27)$$

From this, we get  $D(0) = 2.22$  and  $D(\infty) = 3.19$ , which agrees well with  $D(0) = 2.12$  and  $D(\infty) = 2.98$  reported in [11].

The smooth reduction of the dimension of the spacetime at shorter scales is one of the most interesting features of the CDT model. This is an indication of the highly non-classical behavior at small scales. The reduction in dimension for larger  $\sigma$  is due to the finite (and rather small) volume of the spacetimes being considered.

The spectral dimension vs step size plot for a (3+1)-dimensional spacetime is shown in figure 9. The spectral dimension in this case ranges from a value of about 1.8 at short scales up to a value of about 4.0 at larger values of  $\sigma$ , and then starts to fall for  $\sigma$  greater than about 600, with the functional form being given by:

$$D(\sigma) = 4.43 - \frac{375}{141 + \sigma} \quad (28)$$

This is to be compared with the

$$D(\sigma) = 4.02 - \frac{119}{54 + \sigma} \quad (29)$$

reported in [4].

### 4.3 Spectral Dimension of the Spatial Slices

The spectral dimension of a spatial slice can be computed using a process identical to that used for determining the spectral dimension of the full spacetime. We select the slice with the maximum

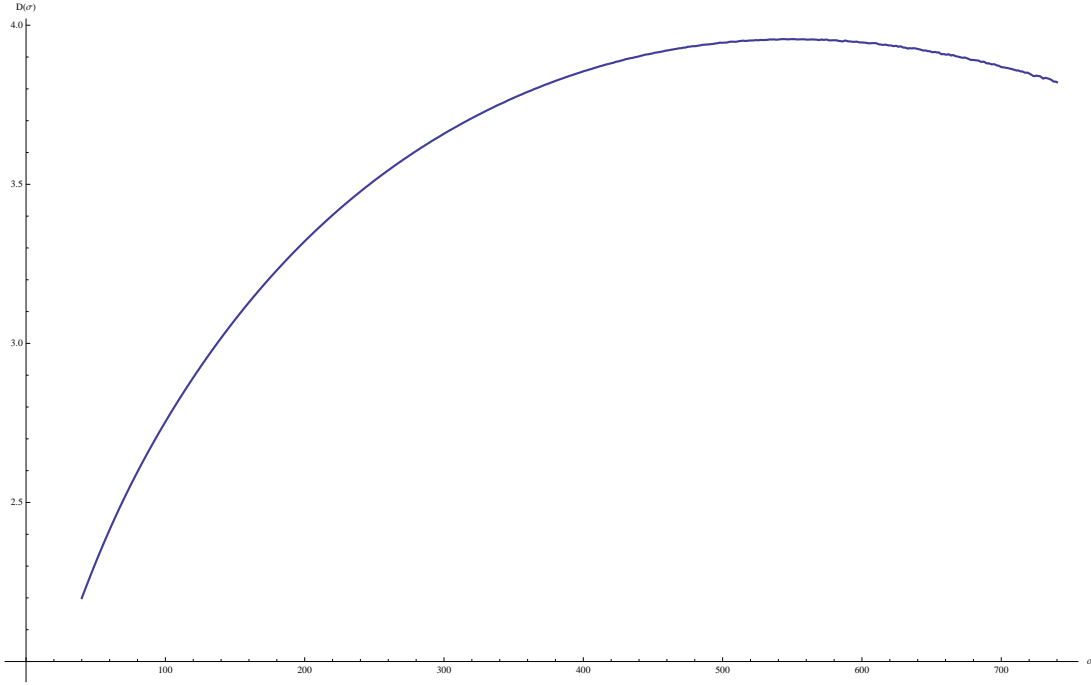


Figure 9: Spectral dimension for a (3+1) spacetime vs  $\sigma$ ,  $N_4 = 80000$ ,  $\kappa_0 = 3.6$ ,  $\Delta = 0.6$

$(d - 1)$ -volume and initiate diffusion processes from a randomly selected  $(d - 1)$ -simplex on this slice.

The spectral dimension of the maximum volume slice for a (3+1)-dimensional spacetime is shown in figure 10. For short scales, up to  $\sigma \approx 40$ , the return probability differs considerably for even and odd step sizes, and the plot bifurcates. Once the even and odd step size spectral dimensions converge,  $D(\sigma)$  is approximately 1.5, before a gradual reduction due to finite size scaling. In [4], a spatial slice spectral dimension of 1.56 is reported. This value is computed by calculating the average return probability of all the spatial slices. The agreement of our results with value reported in [4] indicates that each spatial slice has roughly the same spectral dimension.

Figure 11 shows a corresponding plot for (2+1)-dimensional spacetime. In this case, the even and odd  $\sigma$  plots converge at a much larger value of  $\sigma \approx 150$ . The spectral dimension value then levels off at about 1.65

## Volume Profile

At the beginning of this section, we discussed the emergence of an extended phase, which we said was a solution to the classical Einstein equations. However, the only evidence we have presented so far are figures 3 and 7, where the shape of the volume profile is indicative of such a solution. There is a rigorous, quantitative procedure, in which volume profiles of the spatial slices are fit to the Euclidean de Sitter solution, in 2+1 and 3+1 dimensions. This procedure is described in detail in [14]. We have been able to verify these results in 2+1 and 3+1 dimensions; our analysis will be presented in [5].

## 5 Conclusions

The Causal Dynamical Triangulations approach to quantum gravity has many promising features, and our computer simulation has been able to successfully reproduce these results in 2+1 and 3+1

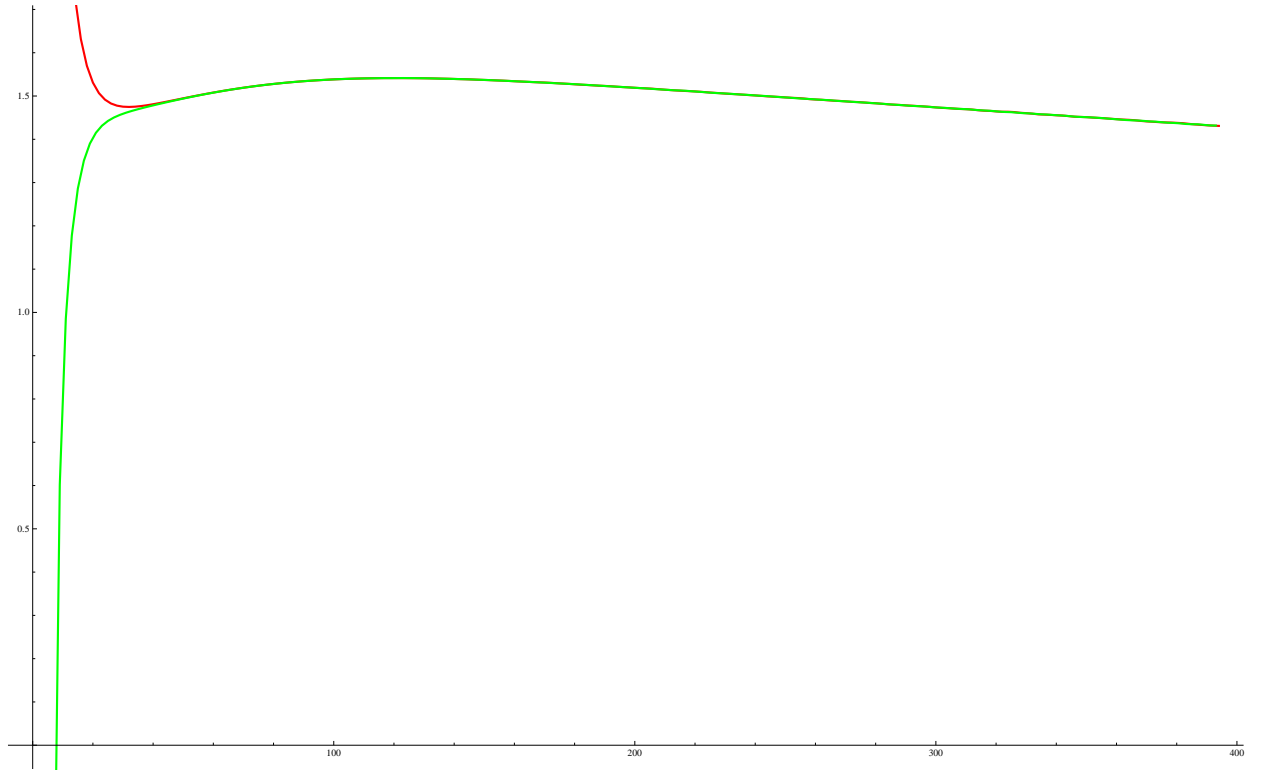


Figure 10: Spectral dimension for the maximum volume spatial slice for a 3+1 spacetime

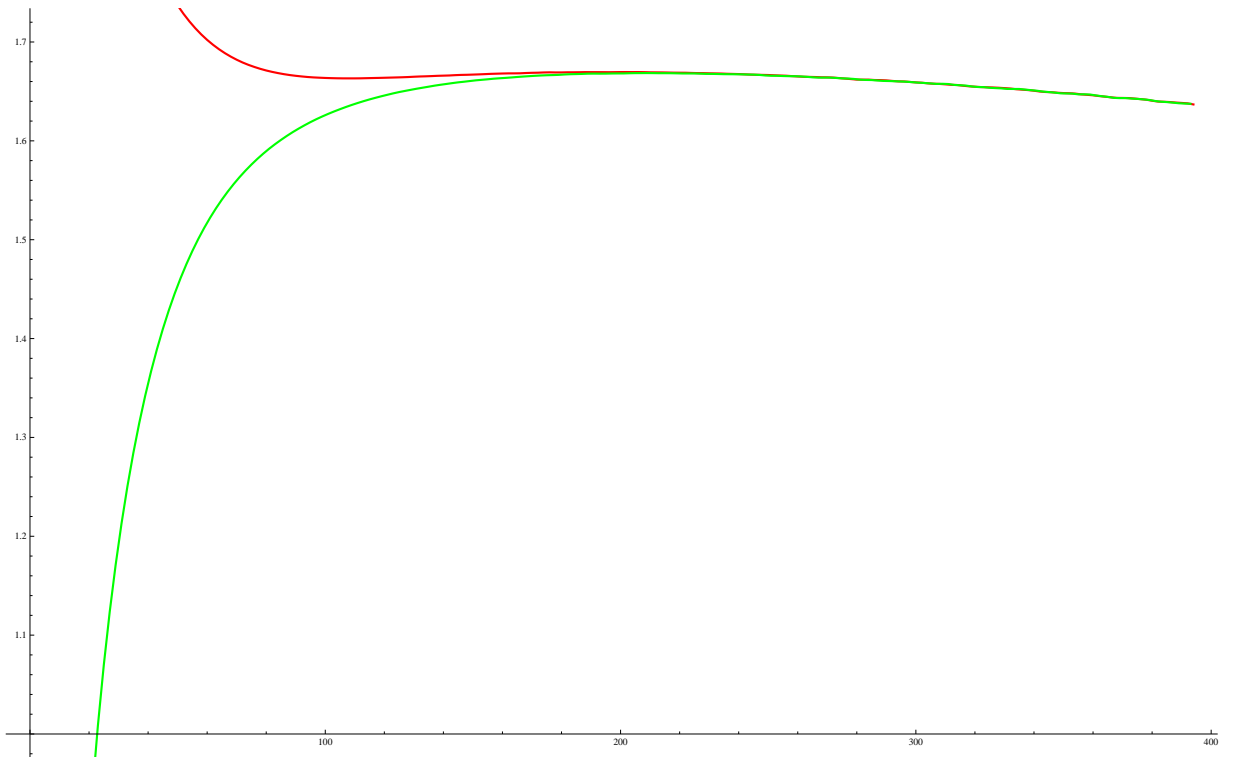


Figure 11: Spectral dimension for the maximum volume spatial slice for a 2+1 spacetime

dimensions. Most of these results were first reported by Ambjørn, Jurkiewicz, and Loll [1, 2, 3, 4], and our simulation provides the first completely independent verification. We observe the emergence of a well defined extended geometric phase. This geometric phase shows a smoothly changing spectral dimension that ranges from a value close to 2.0 to a value larger than 3.0 for the (2+1)-dimensional spacetimes and from about 2.0 to 4.0 for the (3+1)-dimensional spacetimes. The spatial slices exhibit a non-classical behavior, as indicated by their spectral dimension plots.

Our successful reproduction of many of the results reported by Ambjørn, Jurkiewicz, and Loll, using a completely independent software implementation, should improve confidence in the CDT model. With the exception of the value of the phase transition point in the (2+1)-dimensional model, our results are in good agreement with those reported in [3, 4, 14], and convince us of the overall validity of the CDT approach.

Having successfully reproduced the basic results of the CDT model, we are now using our CDT implementation to explore some further interesting problems. These include investigating the quantum fluctuations in (2+1)-dimensional CDTs and comparing the results with canonical quantization approaches [6], detailed analysis of the volume profiles in 2+1 and 3+1 dimensions [5] and exploring Horava-Lifshitz gravity on the CDT lattice [7]. In the near future, we plan to release our implementation into the public domain.

## Acknowledgements

I would like to thank Professor Steve Carlip for his initial suggestion of CDT as a research topic, and for his guidance and patience for the duration of this project. I would like to thank the summer REU students, Jun Zhang, Masha Baryakhtar, David Kamensky and Christian Anderson, for their valuable contributions to the project. I would also like to thank Joshua Cooperman, Adam Getchell, Michael Sachs and Patrick Zulkowski for helpful discussions regarding CDT and for their willingness to work with poorly documented code written in an unfamiliar programming language.

This work was supported in part by DOE grant DE-FG02-91ER40674.

## References

- [1] J. Ambjørn, J. Jurkiewicz, and R. Loll, *Nonperturbative Lorentzian path integral for gravity*, *Phys. Rev. Lett.* **85**, 924 (2000)
- [2] J. Ambjørn, J. Jurkiewicz, and R. Loll, *Dynamically triangulating Lorentzian quantum gravity*, *Nucl. Phys. B* **610**, 347 (2001)
- [3] J. Ambjørn, J. Jurkiewicz, and R. Loll, *Nonperturbative 3D Lorentzian quantum gravity*, *Phys. Rev. D* **64**, 044011 (2001)
- [4] J. Ambjørn, J. Jurkiewicz, and R. Loll, *Reconstructing the universe*, *Phys. Rev. D* **72**, 064014 (2005)
- [5] J. Cooperman, *Further evidence for the emergence of de Sitter spacetime from Causal Dynamical Triangulations*, in preparation.
- [6] M. Sachs, *Testing lattice quantum gravity in 2+1 dimensions*, arXiv:1110.6880 [gr-qc]
- [7] C. Anderson, S. J. Carlip, J. H. Cooperman, P. Horava, and P. Zulkowski, *Quantizing Horava-Lifshitz Gravity a la Causal Dynamical Triangulations*, in preparation.
- [8] T. Regge, *General relativity without coordinates*, *Il Nuovo Cimento (1955-1965)* **19**, 558 (1961)

- [9] N. Metropolis, A. W. Rosenbluth, M. N. Rosenbluth, A. H. Teller and E. Teller, *Equation of state calculations by fast computing machines*, *J. Chem. Phys.* **21**, 1087 (1953)
- [10] J. Ambjørn, J. Jurkiewicz, and R. Loll, *The spectral dimension of the universe is scale dependent*, *Phys. Rev. Lett.* **95**, 171301 (2005)
- [11] D. Benedetti and J. Henson, *Spectral geometry as a probe of quantum spacetime*, *Phys. Rev. D* **80**, 124036 (2009)
- [12] S. Carlip, *The small scale structure of spacetime*, arXiv:1009.1136 [gr-qc]
- [13] J. Ambjørn, J. Jurkiewicz, and R. Loll, *The universe from scratch*, *Contemporary Physics* **47**, 103 (2006)
- [14] J. Ambjørn, J. Jurkiewicz, and R. Loll, *Nonperturbative quantum de Sitter universe*, *Phys. Rev. D* **78**, 063544 (2008)